Carbon Letters (2023) 33:1145–1160
https://doi.org/10.1007/s42823-023-00487-2

Online ISSN 2233-4998
Print ISSN 1976-4251

ORIGINAL ARTICLE

Synthesis, characterization and evaluation of porous carbon adsorbents derived from waste biomass for CO_2 capture

Dosali Mallesh[1,2] · Shobanaboyina Swapna[1,2] · Paka Rajitha[1,2] · Yarasi Soujanya[1,2] · Chenna Sumana[1,2] · Nakka Lingaiah[1,2]

Received: 3 September 2022 / Revised: 16 February 2023 / Accepted: 21 February 2023 / Published online: 21 March 2023

Abstract
In this work, subabul wood biomass was used to prepare carbon adsorbents by physical and chemical activation methods at various carbonization temperatures. The properties of the carbon adsorbents were estimated through characterization techniques such as X-ray diffraction, Fourier transform infrared spectroscopy, X–ray photo electron spectroscopy, laser Raman spectroscopy, scanning electron microscopy, CHNS-elemental analysis and N_2 adsorption studies. Subabul-derived carbon adsorbents were used for CO_2 capture in the temperature range of 25–70 °C. A detailed adsorption kinetic study was also carried out. The characterization results indicated that these carbons contain high surface area with microporosity. Surface properties were depended on treatment method and carbonization temperature. Among the carbons, the carbon prepared after treatment of H_3PO_4 and carbonization at 800 °C exhibited high adsorption capacity of 4.52 m.mol/g at 25 °C. The reason for high adsorption capacity of the adsorbents was explained based on their physicochemical characteristics. The adsorbents showed easy desorption and recyclability up to ten cycle with consistent activity.

Keywords Subabul wood · Carbon dioxide · Activated carbon · Adsorption · Carbonization

1 Introduction

One of the main greenhouse gases, CO_2, is responsible for disturbing the cycle of normal climate conditions. It is a major contributor toward global warming. The main source for the accumulation of CO_2 in the atmosphere is by combustion of fossil fuels and deforestation. The present and expected future demand for global energy suggests that it is impossible to reduce the utilization of fossil fuels. There is a need to stabilize the climate changes by controlling CO_2 emission. In the twenty-first century, global climate change due to the rise of CO_2 in the atmosphere has become one of the important environmental and energy concerns [1]. Therefore, to reduce the CO_2 level in the atmosphere, carbon capture technologies are the major optional methods [2, 3].

Various activation methods were developed for CO_2 capture such as physical [4, 5], chemical [6–8] and membrane technology [9–11]. Among these methods, adsorption by using solid adsorbents is the prominent approach due to the requirement of low energy, low cost and easy operation [9, 10, 12, 13]. Solid adsorbents such as metal–organic frameworks [14], zeolites [15], zeolitic imidazole frameworks [16], calcium oxides [17] and supported amines [18] are used for CO_2 capture. The use of these solid adsorbents needs specific techniques and is associated with high cost. Under these conditions, many researchers have focused on the development of solid adsorbents from renewable sources. Waste biomass is a renewable source for synthesis of low-cost solid carbon adsorbents [19]. The solid adsorbents, activated carbons (AC) derived from plant waste biomass, could be low-cost materials and are considered as excellent materials in the adsorption process because of their high specific surface area and pore volume [20, 21]. As materials with high surface area, adequate porosity, and high mechanical strength containing active carbons required, various waste plant materials have been used to prepare these carbons [22]. Activated carbons are prepared in two ways, one by physical activation (CO_2 or steam activation) [23, 24] and the

✉ Nakka Lingaiah
nakkalingaiah@iict.res.in

[1] Department of Catalysis & Fine Chemicals Division, CSIR-Indian Institute of Chemical Technology, Hyderabad, Telangana 500007, India

[2] Academy of Scientific and Innovative Research (AcSIR), Ghaziabad 201002, India

second by chemical activation (KOH, $ZnCl_2$, H_3PO_4, etc.) [25, 26]. The porous carbons were modified using physical and chemical activation processes to create carbon with high surface area and tunable porosity to improve CO_2 adsorption capacity [27]. Carbon is exposed to a flow of steam or CO_2 during physical activation procedures. More reactive carbon atoms are removed from the carbon skeleton during this process, resulting in a larger number of pores, improved surface area and porosity [28]. On the contrary, chemical activation method is frequently carried out through impregnation of the carbon with chemical activating agent, followed by carbonization at high temperature at atmospheric condition to form new pores [29]. Among these two methods, chemical activation can lead to generation of high surface area with small pore size materials than the ones prepared by the physical activation method [30].

Many researchers have recently published CO_2 adsorption capability of several biomass-based porous carbon adsorbents under various conditions. For example, Khuong et al. examined CO_2 capture capacity of carbon derived from bamboo and found that the solid residue had a CO_2 adsorption capacity of 3.4 mmol/g at ambient conditions [31]. Yang et al. used KOH to activate coconut shell to produce narrow microporous activated carbons with CO_2 adsorption capability of 4.23 mmol/g [32]. At ambient conditions, carbon produced from corn kernel biomass material had a maximum CO_2 adsorption performance of 3.63 mmol/g [33]. Intan Syafiqah Ismail, et al. published that bamboo-based activated carbon produced from single-step H_3PO_4 activation had a maximum CO_2 absorption of 1.46 mmol/g at ambient conditions [34]. Zubbri et al. found that activating rambutan peels treated with KOH resulted in a higher CO_2 adsorption capacity of 2.78 mmol/g at 30 °C and atmospheric pressure [35]. However, it is required to provide a suitable activated carbon adsorbent for maximum CO_2 adsorption capacity by utilizing waste biomass materials.

In continuation of our effort to prepare carbon-based adsorbents from waste biomass, subabul, a widely grown tree in the tropical region, is used as source for preparation of carbon. The scientific name of the commonly called subabul is *Leucaena leucocephala*. It comes under Fabaceae family and sub-family Mimosoideae [36]. It is also known as white lead tree, jumbay, river tamarind or white popinac. Subabul trees are available abundantly in the world, particularly in the southern (Mexico) and northern America, India and other tropical countries. Subabul is widely used for soil fertility, fencing, firewood, paper industry and fiber.

In the current work, we prepared different types of carbon materials for carbon dioxide capture using subabul stems as biomass raw material. Different carbon materials are prepared by direct carbonization and chemical activated method. The carbon materials were characterized thoroughly and used as adsorbents for selective adsorption of CO_2 under different conditions. The adsorption capacities of these materials were explained based on their properties.

2 Experimental

2.1 Preparation of carbon materials from subabul wood

Subabul wood was procured from local suppliers in Hyderabad, India, and H_3PO_4 was procured from SD Fine Chemicals, India. The procured subabul wood was milled to powder and washed with distilled water, followed by drying in an oven at 100 °C for 12 h. The derived wood powder was divided into different portions. Each portion of the powder was carbonized at different temperatures. The carbonization temperatures varied from 600 to 900 °C under nitrogen flow (40 ml/min) for 4 h. The obtained materials were denoted as SB-600, SB-700, SB-800 and SB-900, where SB indicates subabul wood and the number indicates the carbonization temperature. The second type of adsorbent was prepared by treating the wood powder with H_3PO_4 at room temperature. In this method, the biomass powder was treated with 88% H_3PO_4 solution (1:3 weight ratio) for 4 h. Then the wood mass was washed with distilled water repeatedly to get neutral pH. The solid biomass was kept in an oven for drying overnight at 100 °C and subjected to carbonization at different temperatures in the range of 600–900 °C. These samples are denoted as SBPA-600, SBPA-700, SBPA-800 and SBPA-900, where SBPA stands for subabul treated with H_3PO_4 and the number indicates the carbonization temperature.

2.2 Characterization

BET surface area of the adsorbents was measured from N_2 adsorption–desorption data acquired on BELSORB II Instrument, Japan. Powder X-ray diffraction (XRD) patterns of the adsorbents were recorded on Rigiku Miniflex (Rigaku Corporation, Japan) X-ray diffractometer using Ni filtered CuK_α radiation ($\lambda = 1.5406$ Å) in the scan range of 10–80°. FT-IR spectra of the samples were obtained on FT-IR DIGILAB Biorad spectrometer using a KBr disc method. C, H, N and S elemental analysis was carried out on a Vario Micro Cube elemental analyzer. Raman spectra of carbon adsorbents were analyzed with Horiba JobinYvon LabRAM HR spectrometer. Thermo Scientific K-ALPHA surface analysis spectrometer was used to obtain X-ray photoelectron spectra (XPS) using a monochromatic, micro-focused Al–Ka radiation (1486.6 eV). SEM images of the adsorbents were obtained on a JEOL FE-SEM-7610F microscope. The detailed procedure of all characterization techniques was presented in our previous publication [37].

2.3 Carbon dioxide adsorption measurements

CO_2 adsorption studies were conducted in a dynamic adsorption flow system. The adsorption was performed in a fixed bed reactor (SS, 41 cm length: 0.9 cm id). In a typical experiment, about 1 g of carbon adsorbent was mixed with 0.5 g of quartz beads suspended in the middle of the reactor between two quartz plugs and pretreated under helium atmosphere at 200 °C for 1 h. Helium was passed through the reactor bed at the required flow rate with the help of mass flow controllers for removal of moisture content present on the adsorbent. 10% CO_2 balance He gas mixture was passed over the adsorbent at the desired temperature (25–70 °C) and the gas concentration was monitored at the outlet periodically. After the sample had attained its CO_2 saturation capacity, it was purged with He gas for 30 min. The outlet gas was analyzed online using a gas chromatograph (Agilent Technologies 7820A equipped) equipped with a thermal conductivity detector and a Porapak Q column. The adsorption data were collected at three different temperatures (25, 50 and 70 °C). Then the adsorption sample was flushed with pure helium gas for 30 min and desorption was carried out by increasing the temperature at a rate of 5 °C/min until it reached 160 °C.

2.4 CO_2 adsorption kinetics

In the present study, the kinetic analysis of CO_2 adsorption is evaluated at different temperatures (i.e., 25 °C, 50 °C and 70 °C) based on pseudo-first-order, pseudo-second-order and Avrami fractional order kinetic models.

Pseudo-first-order kinetic model assumes that the rate of adsorption is proportional to the number of available active sites on the adsorbent. The integrated form of the models is expressed as:

$$Q_t = Q_e(1 - \exp(-k_f t),$$

where Q_t and Q_e are the amount of CO_2 adsorbed for unit mass of adsorbent (mmole/g) at any time, t, and at equilibrium, respectively, and k_f (min^{-1}) is the rate constant.

In pseudo-second-order kinetic model, the rate of adsorption is proportional to the square of number of free active sites on the adsorbent. The integrated form is given by:

$$Q_t = \frac{Q_e^2 k_s t}{1 + Q_e k_s t},$$

where k_s (g $mole^{-1}$ min^{-1}) is the second-order rate constant.

Avrami fractional order kinetic model is expressed as follows:

$$Q_t = Q_e\left[1 - \exp(-(k_A t)^{n_A})\right],$$

where k_A (min^{-1}) is the Avrami kinetic constant and n_A is the Avrami exponent.

The accuracy of the model is evaluated based on the coefficient of determination (R^2) and is expressed as follows:

$$R^2 = 1 - \frac{\sum_{i=0}^{n}\left(Q_{t(exp)} - Q_{t(model)}\right)^2}{\sum_{i=0}^{n}\left(Q_{t(exp)} - \overline{Q_{t(exp)}}\right)^2},$$

where $Q_{t(exp)}$ and $Q_{t(model)}$ are experimental and calculated values of CO_2 absorbed. $\overline{Q_{t(exp)}}$ is the average value of experimental data. n represents the total number of experimental data points.

Once the kinetic parameters are calculated for the best model, the activation energy is evaluated using rate constant (k) at different temperatures based on Arrhenius equation.

$$k = k_0 e^{-E/RT},$$

where k_0 is the Arrhenius pre-exponential factor, E is the activation energy (cal $mole^{-1}$), R is the universal gas constant (cal $mole^{-1}$ K^{-1}) and T is the temperature (K).

3 Results and discussion

3.1 Characterization of carbon adsorbents

The N_2 adsorption–desorption data were used to determine the specific surface area and porosity of the adsorbents. The isotherms of SB and SBPA carbon adsorbent materials are presented in Fig. 1. The pore size distributions are shown in Fig. 2. According to IUPAC classification, type I isotherm was observed for SB and SBPA carbon adsorbents. Among these, SB carbon adsorbents showed hysteresis loop with type I isotherm, which indicates that the carbons have more micropores and less mesopores. The SB-800 and SB-900 samples not only show type I, but also type IV isotherm with H4-type hysteresis loop associated with monolayer—multilayer adsorption condensation in narrow slit-like pores [38]. SBPA carbons showed type I isotherm and exhibited high nitrogen uptake at low relative pressure ($P/P_0 < 0.1$) associated with the microporous structure. SBPA-800 and SBPA-900 samples have narrow micropores with < 1 nm pore size. These SBPA adsorbents exhibited an identical sharp knee associated with similar microporosity [39]. The textural properties of the adsorbents are shown in Table. 1. The surface area and pore volume of the carbons were increased with carbonization temperature from 600 to 900 °C for both SB and SBPA samples. As the carbonization temperature was increased from 600 to 900 °C, both surface area and pore volumes of the activated carbons increased

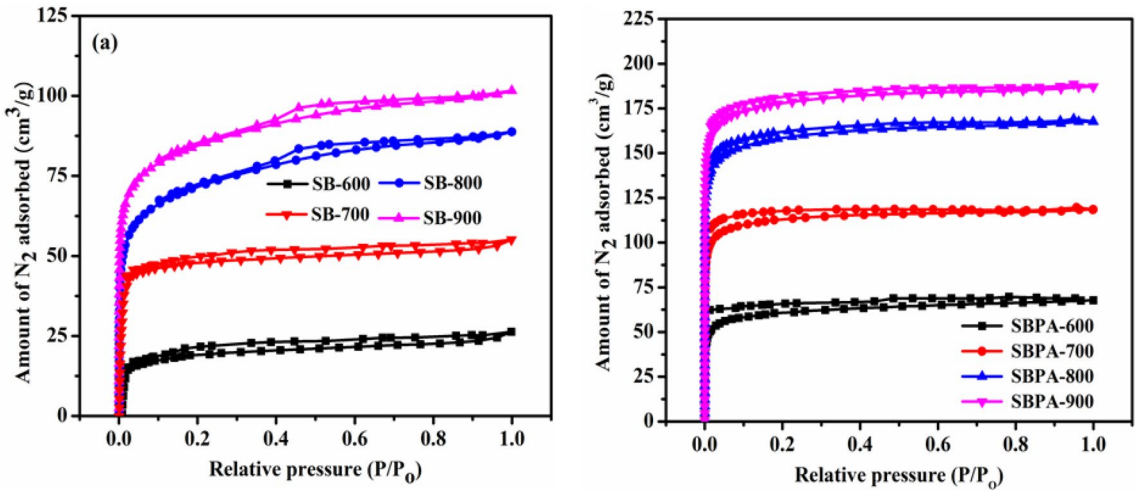

Fig. 1 N_2 adsorption–desorption isotherms of **a** SB samples and **b** SBPA samples

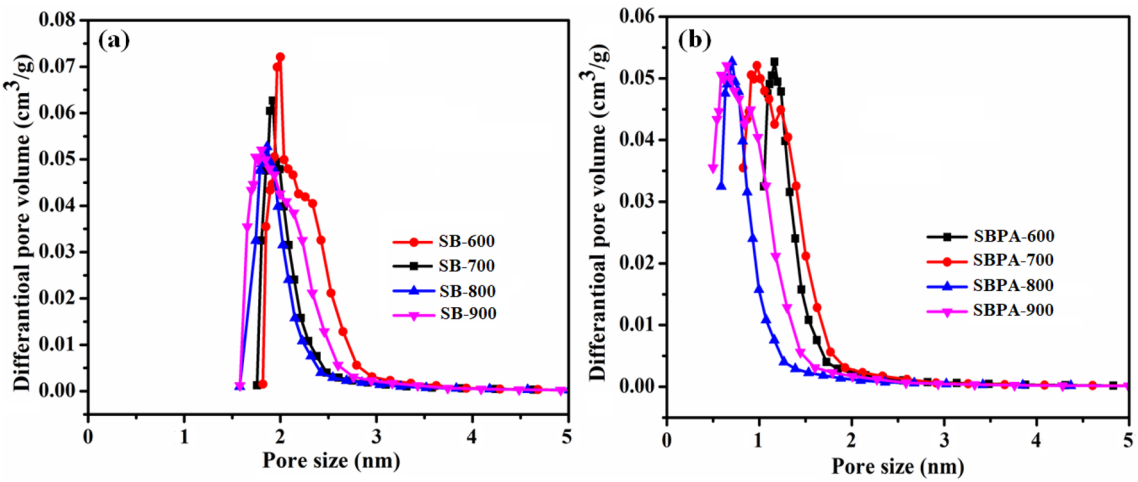

Fig. 2 Pore size distribution of **a** SB samples and **b** SBPA samples

Table 1 Textural properties of the activated carbons

Adsorbent	S_{BET} [a] (m^2/g)	S_{micro} [b] (m^2/g)	V_{micro} [c] (cm^3/g)	V_{meso} [d] (cm^3/g)	V_p [e] (cm^3/g)	D_p [f] (nm)
SB-600	57	10	0.01	0.04	0.05	2.24
SB-700	248	219	0.06	0.02	0.08	2.05
SB-800	397	320	0.11	0.09	0.20	1.94
SB-900	528	465	0.15	0.10	0.25	1.87
SBPA-600	387	343	0.09	0.07	0.16	1.25
SBPA-700	576	528	0.13	0.08	0.21	1.08
SBPA-800	823	718	0.17	0.09	0.26	0.85
SBPA-900	905	821	0.16	0.11	0.27	0.83

"[a]Surface area calculated using BET method. [b]Micropore surface area from *t*-plot method. [c]Micropore volume determined by the *t*-plot method. [d]Mesopore volume determined from V_p —V_{micro}. [e]Total pore volume at $P/P_0 \sim 0.99$. [f]Average pore diameter "

due to thermal degradation and the volatilization process of the impregnated H_3PO_4 present in the biomass [38]. In SBPA carbons, temperature rise also led to the generation of a large volume of narrow micropores.

The XRD patterns of the activated carbons are presented in Fig. 3. The results mainly showed two characteristics peaks at 2θ of 24.2° and 42.6°. These two broad peaks are recognized by the presence of partial multilayered graphitic domains corresponding to the reflection planes of (0 0 2) and (1 0 1) [40, 41]. However, when the carbonization temperature rose from 600 to 900 °C, the position of the XRD peak at 2θ = 24.2° shifted toward a higher degree. This shift suggests that, due to thermal effect at high temperature regions, a reduction in the interlayer distance of the graphite structure as well as the loss of linking functional groups [10, 42]. Nevertheless, after H_3PO_4 treatment, the XRD peaks at 2θ of 24.2° and 42.6° are at high intensity than those of SB carbons, indicating that presence of more graphitic structure. However, the peak intensity at 2θ = 42.6° of SBPA carbons was decreased with increase in carbonization temperature from 600 to 900 °C. It indicates that during the carbonization process, a greater degree of chemical reaction between H_3PO_4 and biomass components ensues, resulting in a much higher number of defects in the synthesized activated carbons [38, 42].

Laser Raman spectra of the activated carbons are presented in Fig. 4. The carbon adsorbents showed distinct peaks at 1329 and 1595 cm^{-1} corresponding to the D and G bands of the carbon structure [43, 44]. Naturally, the D band is attributed to amorphous or disordered carbons and

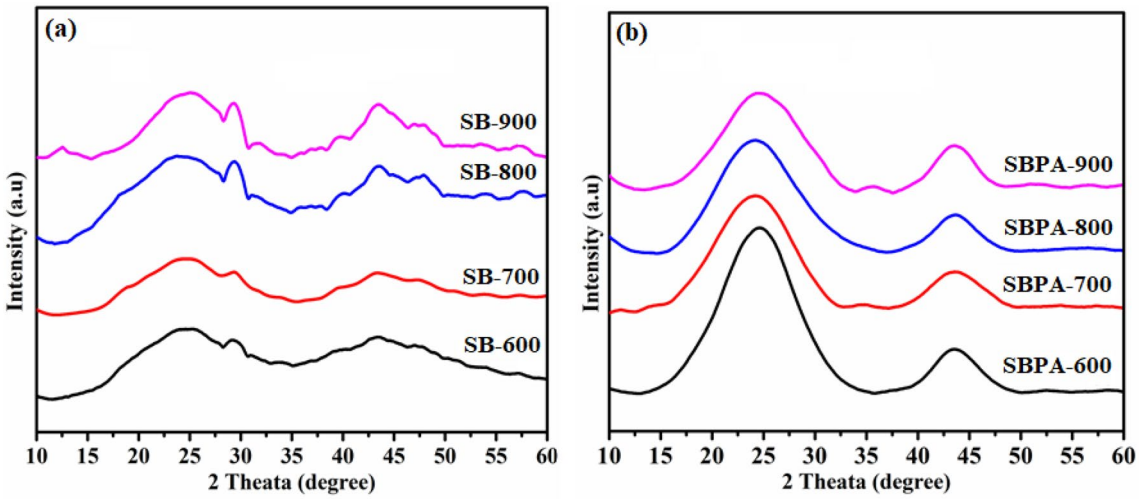

Fig. 3 XRD patterns of **a** SB and **b** SBPA samples

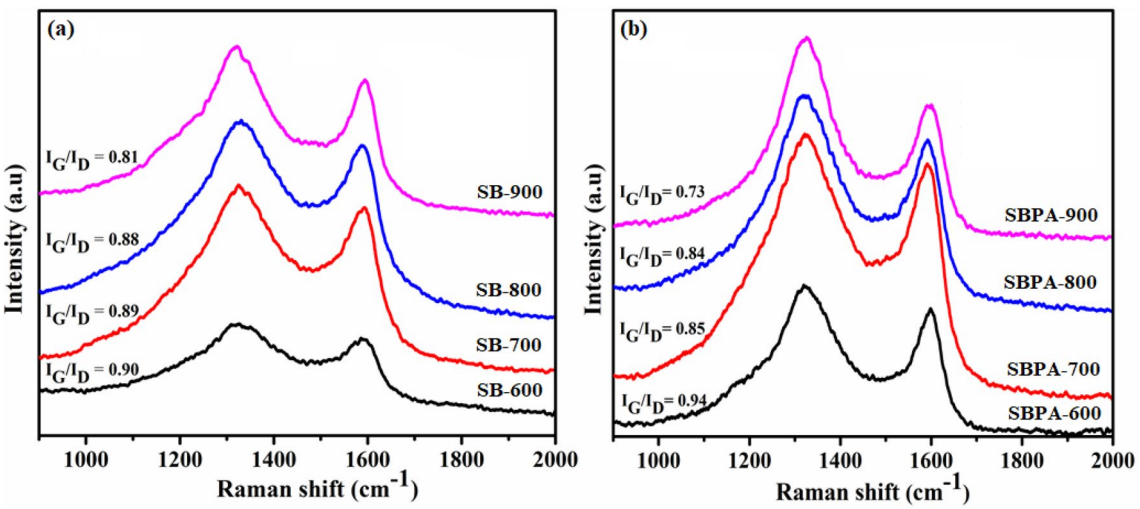

Fig. 4 Raman spectra of **a** SB samples and **b** SBPA samples

the G band suggests the in-plane tangential stretching of C = C bonds in graphene sheets. The degree of graphitization of SB and SBPA carbons was calculated from the intensity ratio of the D and G band. The higher the I_G/I_D ratio, suggesting a higher degree of graphitization, the smaller is the I_G/I_D ratio, suggesting a lower degree of graphitization. The SB and SBPA carbons showed I_G/I_D ratio lower than 1. On increasing the carbonization temperature, the I_G/I_D ratio was decreased from SB-600 (0.90) to SB-900 (0.81) and SBPA-600 (0.94) to SBPA-900 (0.73), suggesting that the degree of graphitization was decreased. In SBPA carbon's increase in carbonization temperature, the I_G/I_D ratio was decreased, suggesting that a greater number of structural defects increased in the samples with low graphitization. This result is in good agreement with XRD and pore size distribution analysis [45, 46].

FT-IR spectra of carbon samples are depicted in Fig. 5. A common band at 3325 cm^{-1} was noticed for SB and SBPA activated carbons corresponding to the –O–H stretching vibration of the adsorbed water. In addition, the SB carbons also exhibited different bands at 2762, 1617, 1419, and 1053 879 cm^{-1}. The band at 2762 cm^{-1} corresponds to asymmetric C–H stretching vibrations. The FT-IR bands observed at 1617 and 1419 cm^{-1} are related to the C = N stretching vibrations of the carbon material [47]. The peaks appearing at 1053 cm^{-1} and 879 cm^{-1} could be assigned to acyclic C–O–C groups, which are conjugated to the C = C and C–S functional groups, respectively [4, 48]. From Fig. 5(a), the band appeared at 1617 cm^{-1} with high intensity for SB-800 carbon, indicating the presence of a greater number of C = N functional groups [25, 47]. SBPA activated carbons showed bands at 2167, 1689, 1134 and 786 cm^{-1}. The FTIR spectra of the activated carbons showed a 2167 cm^{-1} absorption band associated with axial deformation present in triple bonds or accumulated double bonds. These bonds probably occurred due to the presence of carboxylic groups in the activated carbon surface [49, 50]. The strong band appeared at 1689 cm^{-1} ascribed to C = O stretching vibrations of carboxylic groups [4]. The band appearing at 1134 cm^{-1} could be assigned to the hydrogen-bonded P = O and P = OOH groups of aromatic carbon. Another band observed at 786 cm^{-1} related to the presence of aromatic substituted aliphatic groups of carbon [51]. The bands appearing at the 1689 and 1134 cm^{-1} intensity were more for the SBPA-800 sample compared to other SBPA activated carbons. These results indicate the presence of a greater number of C = O and O = P–OH functional groups on the carbon adsorbent. Among SBPA activated carbons, the common band intensity at 3325 cm^{-1} was decreased and the band intensity at 1689 and 1134 cm^{-1} was increased compared to SB carbons due to the interaction between H_3PO_4 and biomass during the activation process [52, 53].

The CHNS analyses of SB and SBPA activated carbons are depicted in Table 2. The SB samples contain high carbon content than the SBPA samples. Among the SB carbons, the percentage of C and N contents decreased and at the same time H and O percentages increased with increase in carbonization temperature. With increase in carbonization temperature, the polymeric structure of biomass (lignin, cellulose and hemicelluloses) decomposed and the non-carbon elements such as oxygen and hydrogen were retained. The carbon and nitrogen percentage decreased from 83.43 to 72.02% and 1.28 to 0.97%, respectively, with change in carbonization temperature from 600 to 900 ºC. At the same time, the hydrogen and oxygen percentages increased from 1.73 to 2.14 and 9.02 to 14.38%, respectively [38]. The

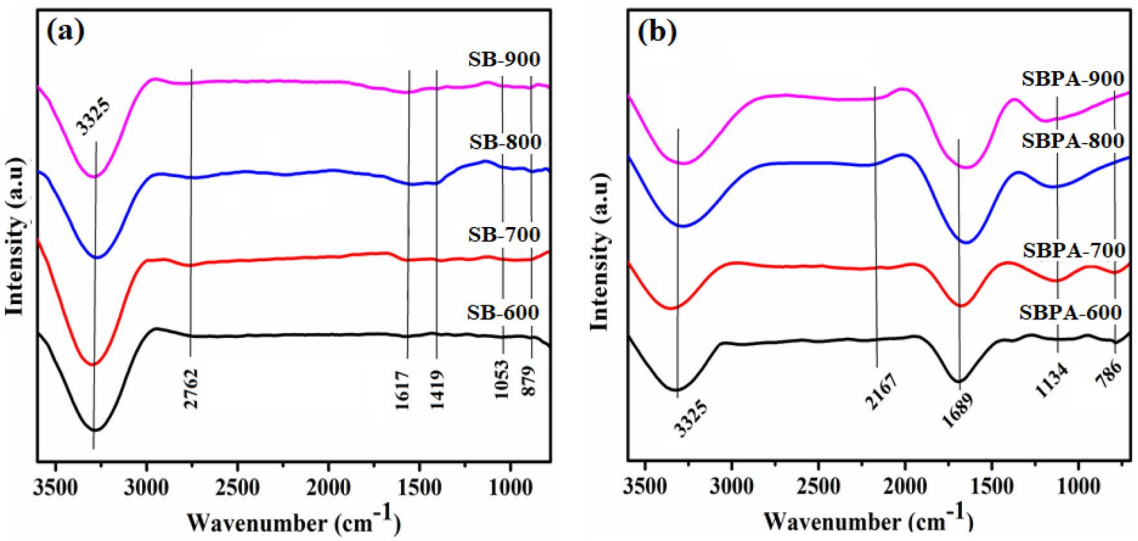

Fig.5 FT-IR patterns of **a** SB samples and **b** SBPA samples

Table 2 CHNS analysis of SB and SBPA activated carbons

Adsorbent	Carbon (%)	Nitrogen (%)	Hydrogen (%)	Sulphur (%)	Oxygen (%)
SB-600	83.43	1.28	1.73	0.21	9.02
SB-700	81.22	1.26	1.84	0.16	10.52
SB-800	73.93	1.00	1.85	0.15	12.92
SB-900	72.02	0.97	2.14	0.09	14.38
SBPA-600	71.65	0.85	1.77	0.05	15.22
SBPA-700	70.27	0.74	1.81	0.04	16.50
SBPA-800	65.85	0.60	2.16	0.03	20.51
SBPA-900	59.63	0.33	2.10	0.02	18.56

SBPA samples also showed similar trend with change in carbonization temperature. During the acid activation process, H_3PO_4 might react with biomass and then the volatile matter gets diffused speedily out of the surface. This is the reason for an increase in the loss of carbon content for SBPA carbon samples. The carbon percentage of SBPA samples was decreased from 71.65 to 59.63% and the oxygen percentage increased from 15.22 to 18.56% with increase in carbonization temperature from 600 to 900 ºC. SBPA-900 carbon adsorbent showed less O, H and N content compared to SBPA-800. Further increase in the temperature from 800 to 900 °C caused an increase in the degree of aromaticity [54]. These results are in support of the observations made from Raman and FT-IR analysis.

The surface chemistry of the carbon adsorbents was characterized by X-ray photoelectron spectroscopy. As shown

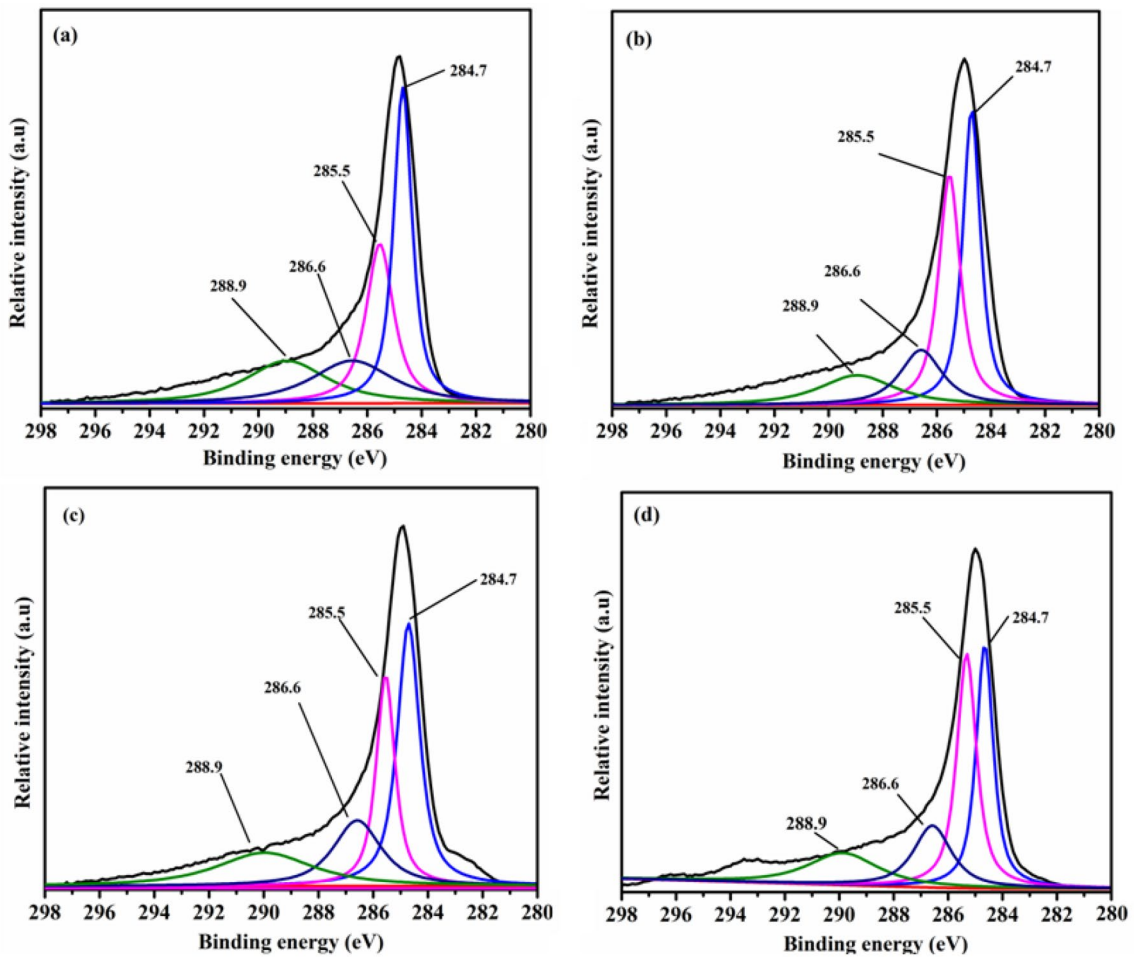

Fig.6 XPS spectra of C1s for SBPA samples: **a** SBPA-600, **b** SBPA-700, **c** SBPA-800 and **d** SBPA-900

in Fig. 6, the deconvoluted C1s XPS spectra of all four activated carbon adsorbents exhibit four different binding energy peaks. The XPS peak at 284.7 eV represents the graphitic carbon, indicating the successful generation of a graphitic structure after treatment with phosphoric acid. In addition, other binding energy peaks at 285.5, 286.6 and 288.9 eV would characterize the presence of carbon in C–OH/C–O–C/C-O-P, carbonyl (-C = O) and the carboxylic/ester/lactone functional groups, respectively [55, 56].

Furthermore, the deconvoluted O1s spectra of all carbon adsorbents exhibit three different binding energy peaks, indicating different types of oxygen functional groups on the surface of the carbon. As shown in Fig. 7, the B.E at around 530.8–531.1 eV represents the carbonyl oxygen in ketone, and the B.E at around 531.9–532.2 eV characterizes the presence of ester and alcoholic oxygen atoms. The third peak at 533.3 eV could be assigned to non-carbonyl anhydride and ester oxygen atoms [4, 57]. Thus, the ketonic functional groups may act as basic sites for the adsorption of CO_2. Moreover, as reported by various studies, it cannot be ruled out that π-electrons in the aromatic ring system of the activated carbon could act as Lewis basic sites for CO_2 adsorption [58].

The atomic percentages obtained from XPS analysis are shown in Table 3. The C and O atomic percentages are in the range from 77.45 to 70.62% and 20.63 to 28.15%, respectively. During the preparation, the increase in the carbonization temperature and H_3PO_4 ratio with biomass results in primary gasification of the surface carbon and formation of additional oxygen groups on the adsorbent surface. In the

Table 3 The elemental percentage of SBPA carbon adsorbents from XPS analysis

Adsorbent	C	O	N	P
SBPA-600	77.45	20.63	0.40	1.52
SBPA-700	74.47	24.20	0.55	0.98
SBPA-800	71.54	27.59	1.26	0.61
SBPA-900	70.62	28.15	0.87	0.36

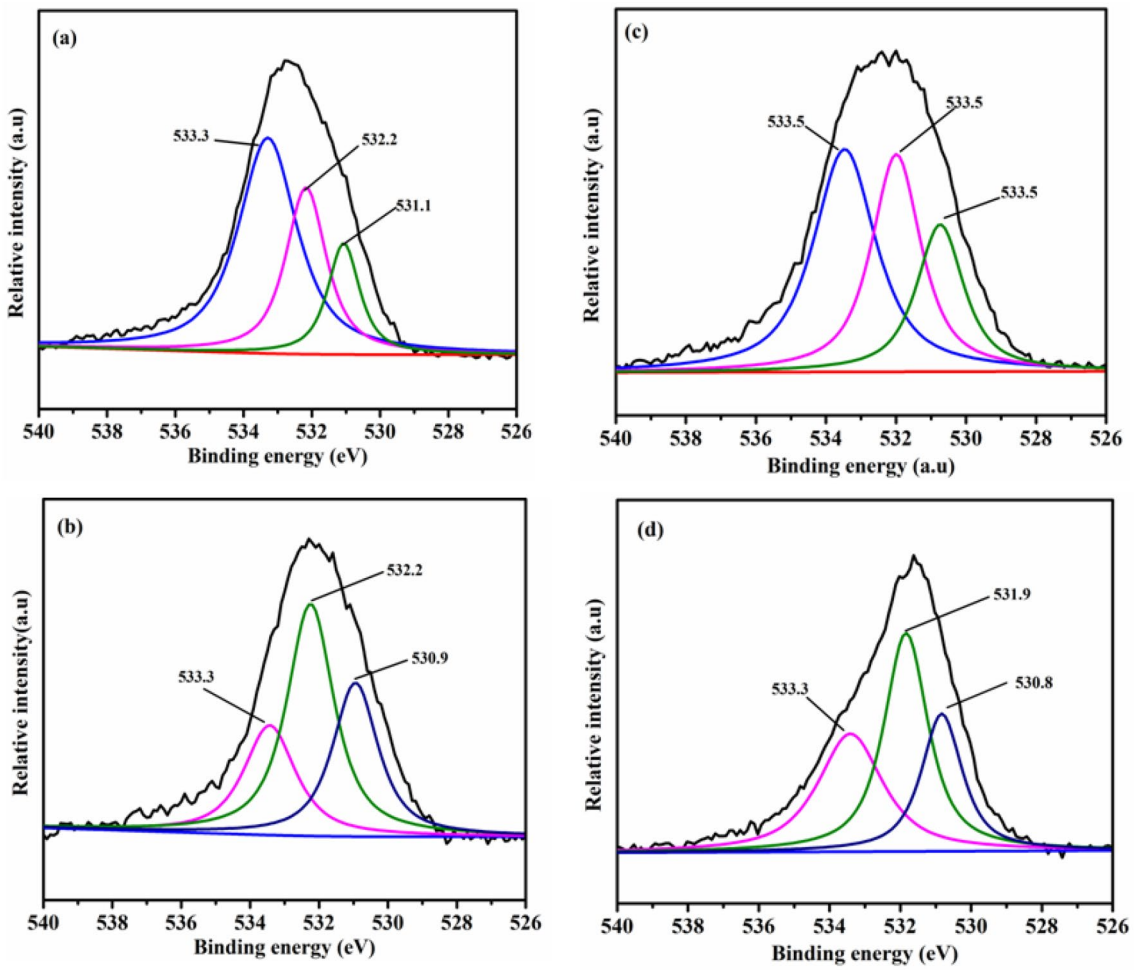

Fig. 7 XPS spectra of O1s for SBPA samples: **a** SBPA-600, **b** SBPA-700, **c** SBPA-800 and **d** SBPA-900

activation process with H_3PO_4, volatile substances diffused fast from the surface and similar findings were reported [38]. The XPS results are in good agreement with the observations made from FT-IR and CHNS analysis.

The morphology of SB and SBPA activated carbons was captured by FE-SEM analysis and the images are depicted in Fig. 8. Among SB carbons, SB-600 carbon showed smooth surface with irregular arrangements and SB-700 carbon showed flake-like structure. The SB-800 and SB-900 samples showed improvement in the pores with irregular arrangements [25]. SBPA carbons showed the development of microporous structure and porosity with increase in the temperature from 600 to 900 °C due to evaporation of H_3PO_4 during carbonization, leaving the space previously occupied by it [59]. This is the reason for the development of porosity as noticed in the SEM images. Among SBPA activated carbons, SBPA-800 showed honeycomb structure with high microporosity and these results are in good agreement with surface area and pore size distribution of the samples.

3.2 CO_2 adsorption capacity over SB and SBPA activated carbons

CO_2 adsorption capacity of SB and SBPA activated carbons was determined in a fixed bed down flow reactor and the adsorption profile estimated by generating breakthrough curves (BTC) for each sample at different temperatures, are presented in Fig. 9. The CO_2 capture capacity was estimated from BTC for each carbon at different temperatures ranging from 25 to 70 °C and the results are presented in Table. 4. The adsorbents were prepared after treatment with H_3PO_4,

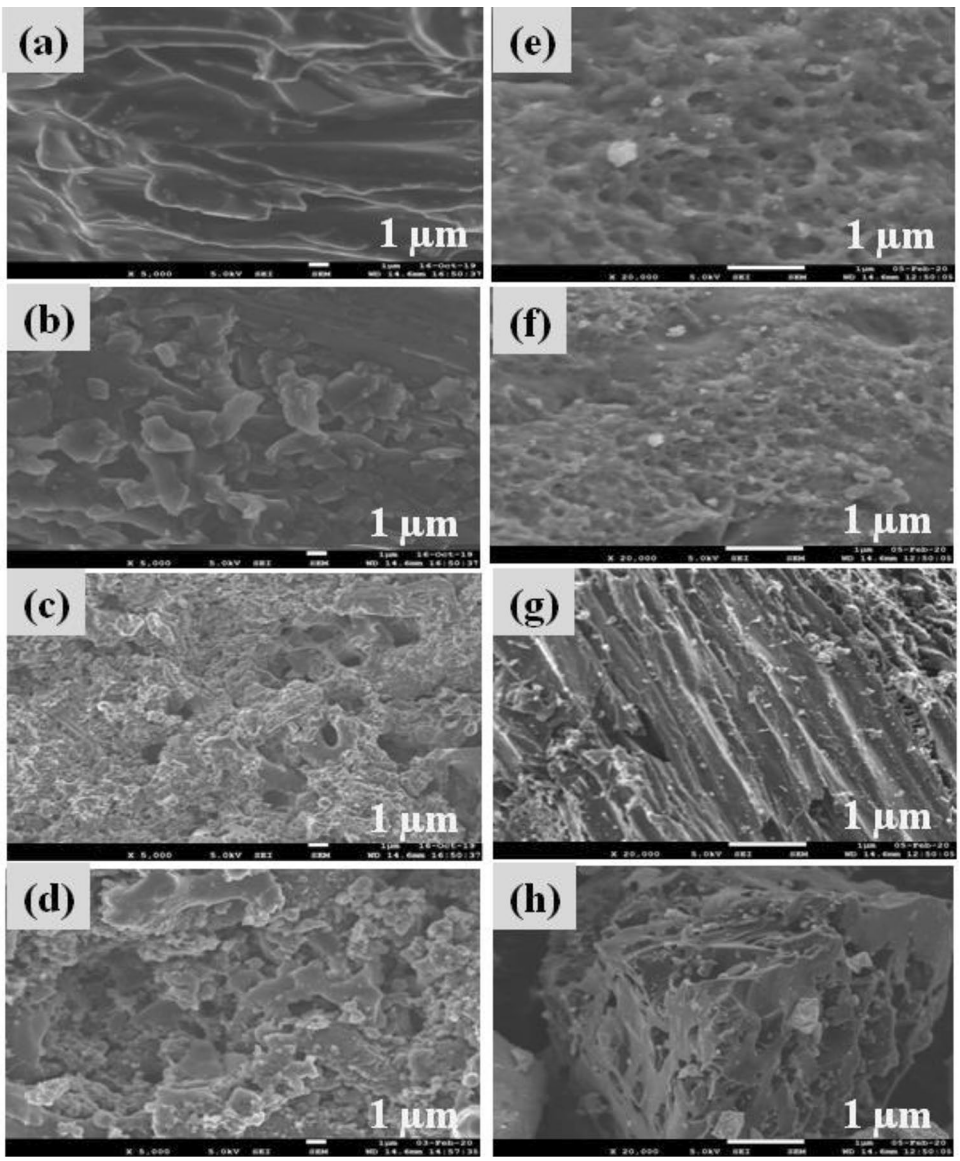

Fig. 8 FE-SEM images of **a** SB-600, **b** SB-700, **c** SB-800, **d** SBPA-900, **e** SBPA-600, **f** SBPA-700, **g** SBPA-800 and **h** SBPA-900

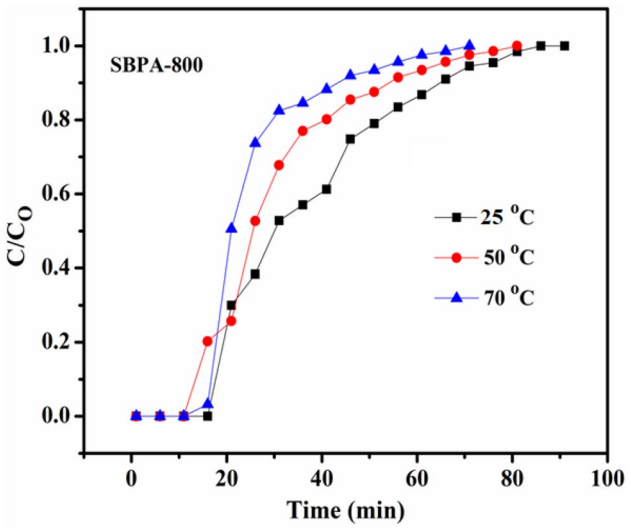

Fig. 9 Breakthrough curves of SBPA-800 activated carbon at different temperatures

Table 4 The CO_2 capture capacities of SB and SBPA activated carbons at different temperatures

Adsorbent	25 °C (m.mol/g)	50 °C (m.mol/g)	70 °C (m.mol/g)
SB-600	1.32	1.08	0.84
SB -700	1.62	1.14	0.92
SB-800	1.84	1.24	1.02
SB-900	2.02	1.62	1.20
SBPA-600	2.50	1.87	1.0
SBPA-700	3.30	2.48	2.04
SBPA-800	4.52	3.70	3.06
SBPA-900	4.27	3.16	2.52

i.e., SBPA samples exhibited high CO_2 adsorption capacity compared to their corresponding SB samples prepared without any treatment.

The CO_2 adsorption capacity was decreased with increase in adsorption temperature from 25 to 70 °C, as the CO_2 capturing process is exothermic in nature. This is the reason for the decrease in the CO_2 capture capacity with increase in temperature. The adsorption capacities can be explained based on their characteristics. The CO_2 adsorption capacity depended on the textural properties of activated carbons, such as surface area, pore volume and pore size distribution.

The adsorbents derived from different raw materials exhibited CO_2 adsorption capacities based on their pore structures. It is reported that the phenolic resin-based carbon spheres with high portion of small micropores (0.8–1.0 nm) showed high CO_2 adsorption capacity under ambient conditions. In another study, carbon derived from polymer spheres treated with KOH contains fine microporosity, which resulted in superior CO_2 adsorption capacity of 4.6 mmol/g at 23 °C [60, 61]. The activated carbon derived from polysaccharides and sawdust biomass treatment with KOH showed high CO_2 capture of 4.8 mmol/g due to the presence of a large number of narrow micropores (< 1 nm) [62]. These studies provided experimental confirmation for the importance of small micropores in CO_2 capture. Thus, the results conclude that high volume of small micropores play an important role for achieving high CO_2 capture under ambient conditions [63]. The CO_2 capture capacity of activated carbon prepared from H_3PO_4-treated cypress sawdust biomass containing micropores showed about 1.73 mmol/g CO_2 adsorption capacity at 25 °C [64]. The CO_2 capture capacity of granular bamboo-derived carbon with narrow micropore (diameter of < 1) showed 4.6 mmol/g [65]. A high CO_2 adsorption was showed by the narrow microporous material, mainly due to the enhancement in the strength of interaction between pore walls and CO_2 molecules. Therefore, to get high CO_2 adsorption capacity, it is imperative to synthesize carbon adsorbents containing narrow micropores [25, 66, 67].

The present carbons prepared after H_3PO_4 showed the presence of reasonable amounts of micropores. As predicted, the carbon adsorbents derived from subabul wood activation using H_3PO_4, followed by carbonization considerably increased the specific surface area from 57 m^2/g to 905 m^2/g and pore volume from 0.05 to 0.27 cm^3/g when compared between SB and SBPA samples. As carbonization temperature increased to 900 °C, the microporosity of the carbon materials improved. Consequently, the mean pore diameter of the pore also decreased close to very narrow micropore range (< 1 nm). Therefore, the low surface area carbon adsorbent SB-600 exhibited lower CO_2 adsorption capacity. Moreover, carbon with microporosity less than 1 nm can capture more amount of CO_2 due to larger adsorption potential [68]. Among these carbons, SBPA-800 carbon showed high CO_2 adsorption capacity of 4.52 mmol/g, as it contains high quantity of micropores (pore size = 0.85 nm and surface area 823 m^2/g). The adsorption capacities of carbon samples not only depended on porosity, but also depend on basic functional groups of nitrogen, oxygen and sulfur present in it [69]. The N-doped carbon prepared from coal-based pitchblende showed maximum CO_2 adsorption capacity of 3.4 mmol/g at 25 °C [70]. The oxygen-functionalized carbon with oxygen percentage of 19.3 showed maximum CO_2 adsorption capacity of 3.9 mmol/g at 25 °C, because of the specific interaction between oxygen functionalities and acidic nature of CO_2 [71]. These results conclude that the basic sites of nitrogen can attract acidic CO_2 more at ambient conditions. The high content of nitrogen, oxygen and sulfur present in SBPA-800 is as shown in Table 2. These

might contribute to its high CO_2 adsorption capacity. When the sulfur is present in the form of oxide (–SO or $–SO_2$, etc.), the negatively charged oxygen might bind with CO_2 and enhance CO_2 capture [25]. These are the reasons for enhanced CO_2 capture at ambient conditions for the present SBPA carbon samples.

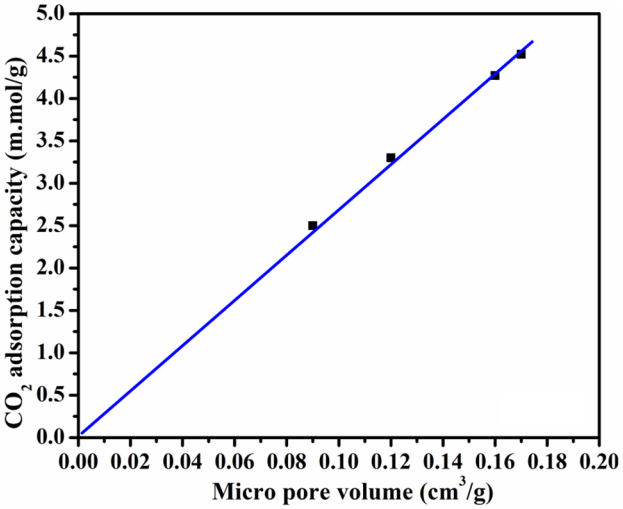

Fig. 10 Relationship between CO_2 adsorption capacity and micropore volume of SBPA samples

Figure 10 indicates the relationship between CO_2 adsorption capacity and micropore volume of the SBPA samples. A linear relationship between micropore volume and CO_2 adsorption capacity was observed. This indicates that CO_2 adsorption capacity increased with increase in the micropore volume. Micropores less than 0.8 nm pore size significantly affects the CO_2 adsorption capacity at low temperature and atmospheric pressure. The reason for these narrow micropores exhibiting the strong adsorption capacity is that they can enhance the strength of interaction between pore walls with CO_2 molecules. Hence, a high CO_2 adsorption capacity was observed with narrow micropores [25]. One can conclude based on the result that SBPA-800 showed high adsorption capacity, mainly because of the presence of narrow micropores.

3.3 Adsorption kinetics

The adsorption kinetic models are developed for SBPA-800 activated carbon of this work using the experimental data collected from CO_2 adsorption studies conducted at three different temperatures (i.e., 25 °C, 50 °C and 70 °C). Figure 11 gives the complete picture of the evaluation of

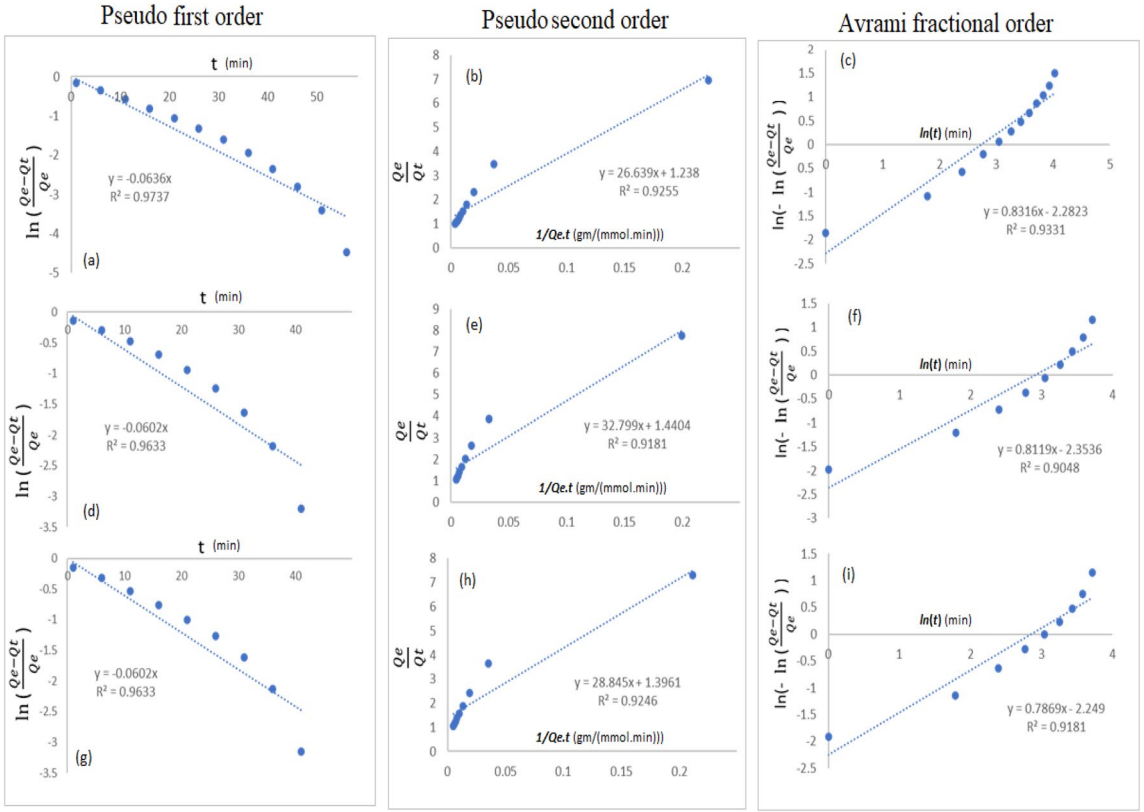

Fig.11 Evaluation of adsorption kinetics from experimental data **a**–**c** at 25 °C, **d**–**f** 50 °C and **g**–**i** 70 °C

adsorption kinetics of all three models: pseudo-first-order, pseudo-second-order and Avrami fractional order kinetic models from experimental data evaluated at 25 °C, 50 °C and 70 °C in Fig. 11 (a–c), Fig. 11(d–f) and Fig. 11 (g–i), respectively. The models are linearized and based on the slope and intercepts of the respective graphs, the kinetic parameters of individual models are generated. The values of kinetic parameters for each model and their corresponding R^2 values are listed in Table 5. It is found that pseudo-first-order kinetic model resulted in relatively high R^2 values for all the temperatures compared to other kinetic models. Therefore, it is concluded that the pseudo-first-order kinetics is the best model to describe the kinetic behavior of CO_2 adsorption. It describes that the adsorption process of SBPA-800 carbon adsorbent is physical adsorption [72, 73], indicating that adsorbed CO_2 was easily desorbed and had stable recyclability. Figure 12 shows the comparison of kinetic models at different temperatures (i.e., 25 °C, 50 °C and 75 °C) with experimental absorption capacity. Further, the activation energy is evaluated using Arrhenius equation by considering the kinetic parameter, k_f, of first-order kinetics at different temperatures and it is found to be 260.0387 cal/mole and thepre-exponential factor k_o is 24.53. The activation energy is Ea > 0, meaning that when the temperature is increased, the reaction rate is increased. This positive Ea value confirms again the physical adsorption with the relatively weak attraction forces.

3.4 Comparison with other carbon adsorbents

The present SBPA-800 activated carbon adsorbent for CO_2 is compared with other adsorbents derived from different biomass sources. The CO_2 capture capacity determined at 25 °C of the reported adsorbents is presented along with that of the present adsorbent in Table 6. Carbon derived from coconut shell and olive stones after carbonization at 800 °C showed less CO_2 adsorption capacity of about 3–3.9 mmol/g than the presented one. The carbon derived from bamboo and other few biomasses showed relatively less or equivalent carbon to SBPA-800. The results show

Table 5 Kinetic parameters for models with corresponding R^2 values for SBPA-800

T (°C)	Q_e (exp)	Pseudo-first order		Pseudo-second order		Avrami kinetics		
		k_f	R^2	k_s	R^2	k_A	n_A	R^2
25	4.491	0.0636	0.9737	0.0375	0.9225	0.0643	0.8316	0.9331
50	5.014	0.0602	0.9633	0.0305	0.9181	0.0551	0.8119	0.9048
70	4.721	0.0602	0.9633	0.0347	0.9256	0.0574	0.7869	0.9181

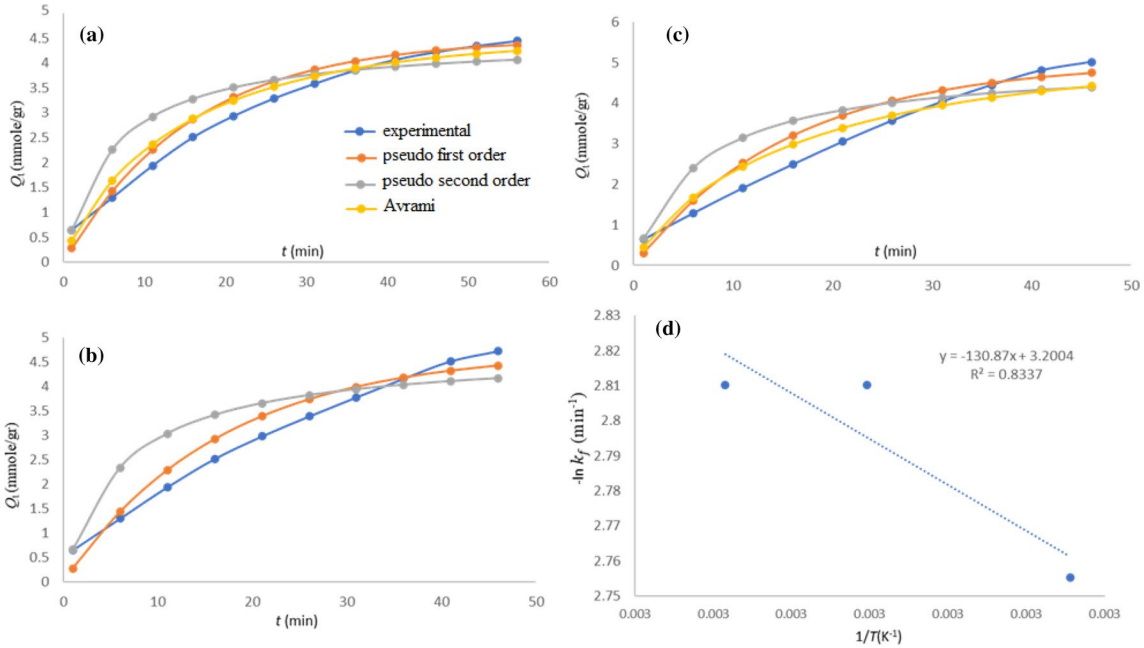

Fig.12 Experimental value of absorption capacity (Q_t) and corresponding fit to the kinetic models with time at temperatures: **a** 25 °C, **b** 50 °C, **c** 70 °C and **d** Arrhenius plot

Table 6 Comparison of activated carbons prepared from different sources for CO_2 capture

Precursor	Carbonization temp. (°C)	Surface area (m^2/g)	Pore volume (cm^3/g)	Average pore diameter (nm)	Adsorption capacity 25 °C (mmol/g)	Reference
Coconut shell	800	1327	0.59	0.8	3.9	[74]
Chestnut	600	607	0.53	6.3	2.3	[75]
Peanut shell	550	1713	0.73	3.3	4.4	[76]
Olive stones	800	1113	0.51	4.8	3.0	[77]
African palm shell	600	1250	0.61	0.92	4.4	[78]
Bamboo	500	1846	0.36	0.8	4.5	[65]
Arundo donax	600	1122	0.59	0.56	3.6	[79]
SBPA-800	800	905	0.27	0.83	4.5	Present work

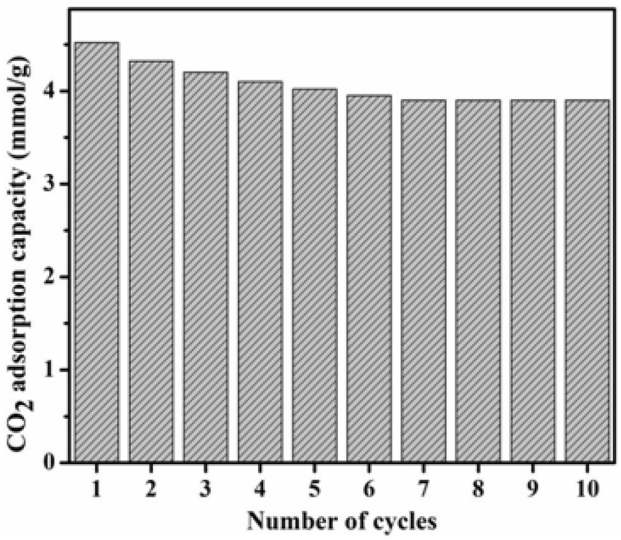

FIG. 13 Recyclability of SBPA-800 activated carbon for CO_2 capture at 25 °C and atmospheric pressure

that the carbons derived from different biomasses exhibited low CO_2 adsorption capacity compared to the present adsorbent derived from subabul wood.

3.5 Recyclability of SBPA-800 activated carbon adsorbent

The SBPA-800 activated carbon adsorbent was tested for its recyclability by conducting adsorption and desorption of CO_2 at 25 °C and 160 °C, respectively and the results are presented in Fig. 11. The CO_2 capture capacity followed by desorption at 160 °C has sustained consequently for ten times. The results show that there is no change in the CO_2 capture capacity during the recycles. A marginal decrease in CO_2 capture capacity for the first six cycles was noticed. Thereafter, the same CO_2 capture capacity was noticed up to ten consecutive Fig. 13 cycles. The results support that the SBPA-800 activated carbon derived after treatment with H_3PO_4 showed not only high capture of CO_2, but also consistent activity on reuse.

4 Conclusions

Summing up, the present research describes the synthesis of low-cost carbon adsorbents from subabul wood with and without treatment at different carbonization temperatures. The carbon adsorbents synthesized with treatment of H_3PO_4 showed high CO_2 capture capacity than the carbons derived without any treatment. The nature of pretreatment of the raw biomass and carbonization temperature directs the surface—structural features of the adsorbents. The carbon derived after acid treatment, followed by carbonization at 800 °C exhibited high CO_2 adsorption of 4.51 mmol/g at ambient temperature and atmospheric pressure. The excellent CO_2 capture ability of carbon derived after acid treatment and carbonization at 800 °C was mainly related to its high surface area (823 m^2/g), micropore volume (0.17 cm^3/g), high content of nitrogen and presence of more basic sites of oxygen functional groups. The present carbon adsorbents derived from subabul exhibited consistent adsorption–desorption of CO_2 up to ten cycles. The CO_2 adsorption process on the SBPA carbon adsorbents follows pseudo-first-order kinetics and the activation energy (Ea) has positive value. These confirm that the adsorption process on SBPA carbons is physical adsorption with the relatively weak attraction forces. Finally, our data imply that SBPA-800 carbon adsorbent could be a feasible CO_2 capture material.

Acknowledgements One of the authors, DM, thanks CSIR, New Delhi, for financial support in the form of Senior Research Fellowship. The authors are thankful to the Director, CSIR–IICT for permission (Communication No: IICT/Pubs./2021/073) to publish the results.

Data availability All data generated or analyzed during this study are included in this published article.

Declarations

Conflict of interest The authors declare that they have no conflict of interest.

References

1. Nurrokhmah L, Mezher T, Zahra A (2013) Evaluation of handling and reuse approaches for the waste generated from MEA-based CO_2 capture with the consideration of regulations in the UAE. Environ Sci Technol 47:13644–13651. https://doi.org/10.1021/es4027198
2. Rochelle GT (2009) Amine scrubbing for CO_2 capture. Science 325:1652–1654. https://doi.org/10.1126/science.1176731
3. Siriwardane RV, Shen MS, Fisher EP, Poston JA (2010) Adsorption of CO2 on molecular sieves and activated carbon. Energy Fuels 15:279–284. https://doi.org/10.1021/ef000241s
4. Heo YJ, Park SJ (2018) H_2O_2/steam activation as an eco-friendly and efficient top-down approach to enhancing porosity on carbonaceous materials: the effect of inevitable oxygen functionalities on CO2 capture. Green Chem 20:5224–5234. https://doi.org/10.1039/C8GC02570C
5. Plaza MG, Pevida C, Arenillas A, Rubiera F, Pis JJ (2007) CO_2 capture by adsorption with nitrogen enriched carbons. Fuel 86:2204–2212. https://doi.org/10.1016/j.fuel.2007.06.001
6. Little RJ, Versteeg GF, Swaaij WPM (1991) Physical absorption into non-aqueous solutions in a stirred cell reactor. Chem Eng Sci 46:3308–3313. https://doi.org/10.1016/0009-2509(91)85036-W
7. Chiesa P, Consonni SP, Eng J (1999) Shift reactors and physical absorption for low-CO_2 emission IGCCs. Gas Turbines Power 121:295–305. https://doi.org/10.1115/1.2817120
8. Aroonwilas A, Veawab A (2004) Characterization and comparison of the CO_2 absorption performance into single and blended alkanolamines in a packed column. Ind Eng Chem Res 43:2228–2237. https://doi.org/10.1021/ie0306067
9. Bishnoi S, Rochelle GT (2000) Absorption of carbon dioxide into aqueous piperazine: reaction kinetics, mass transfer and solubility. Chem Eng Sci 55:5531–5543. https://doi.org/10.1016/S0009-2509(00)00182-2
10. Wei H, Chen J, Fu N, Chen H, Lin H, Han S (2018) Biomass-derived nitrogen-doped porous carbon with superior capacitive performance and high CO2 capture capacity. Electrochim Acta 266:161–169. https://doi.org/10.1016/j.electacta.2017.12.192
11. Harlick PJE, Tezel FH (2004) An experimental adsorbent screening study for CO_2 removal from N_2. Microporous Mesoporous Mater 76:71–79. https://doi.org/10.1016/j.micromeso.2004.07.035
12. Chang FY, Chao KJ, Cheng HH, Tan CS (2009) Adsorption of CO_2 onto amine-grafted mesoporous silicas. Sep Purif Technol 70:87–95. https://doi.org/10.1016/j.seppur.2009.08.016
13. Shahkarami S, Dalai AK, Soltan J (2016) Enhanced CO_2 adsorption using MgO-impregnated activated carbon: impact of preparation techniques. Ind Eng Chem Res 55:5955–5964. https://doi.org/10.1021/acs.iecr.5b04824
14. Zukal A, Dominguez I, Mayerova J, Cejka J (2009) Functionalization of delaminated zeolite ITQ-6 for the adsorption of carbon dioxide. Langmuir 25:10314–10321. https://doi.org/10.1021/la901156z
15. Boehm HP (1994) Some aspects of the surface chemistry of carbon blacks and other carbons. Carbon 32:759–769. https://doi.org/10.1016/0008-6223(94)90031-0
16. Shuren Y, Ding Z, Zhiyong Z, Hai L, Guangjin C, Bei L (2019) A pilot-scale experimental study on CO_2 capture using Zeolitic imidazolate framework-8 slurry under normal pressure. Appl Energy 248:104–114. https://doi.org/10.1016/j.apenergy.2019.04.097
17. Morris W, Leung B, Furukawa H, Yaghi OK, He N, Hayashi H (2011) A Combined experimental-computational investigation of carbon dioxide capture in a series of Isoreticular Zeolitic Imidazolate frameworks. J Am Chem Soc 132:11006–11008. https://doi.org/10.1021/ja104035j
18. Sevilla M, Valle-Vigon P, Fuertes AB (2011) N-Doped polypyrrole-based porous carbons for CO_2 capture. Adv Funct Mater 21:2781–2787. https://doi.org/10.1002/adfm.201100291
19. Vassilev SV, Vassileva CG (2019) Extra CO_2 capture and storage by carbonation of biomass ashes. Energ Convers Manage 204:112331. https://doi.org/10.1016/j.enconman.2019.112331
20. Farha OK, Hupp JT (2010) Rational design, synthesis, purification, and activation of metal-organic framework materials. Acc Chem Res 43:1166–1175. https://doi.org/10.1021/ar1000617
21. Dalai SS, AK, Soltan J, Hu Y, Wang D, (2015) Selective CO_2 capture by activated carbons: evaluation of the effects of precursors and pyrolysis process. Energy Fuels 29:7433–7440. https://doi.org/10.1021/acs.energyfuels.5b00470
22. Lua AC, Guo J (2001) Preparation and characterization of activated carbons from oil-palm stones for gas-phase adsorption. Colloids Surf A 179:151–162. https://doi.org/10.1016/S0927-7757(00)00651-8
23. Plaza MG, Gonzalez AS, Pevida CJ, Pis J (2012) Valorisation of spent coffee grounds as CO_2 adsorbents for post combustion capture applications. Appl Energy 99:272–279. https://doi.org/10.1016/j.apenergy.2012.05.028
24. Boonamnuayvitaya V, Sae-ung S, Tanthapanichakoon W (2005) Preparation of activated carbons from coffee residue for the adsorption of formaldehyde. Sep Purif Technol 42:159–168. https://doi.org/10.1016/j.seppur.2004.07.007
25. Eunji J, Seung W, Choi W, Seok-Min H, Shin S, Lee K (2018) Development of a cost-effective CO_2 adsorbent from petroleum coke via KOH activation. Appl Surf Sci 429:62–71. https://doi.org/10.1016/j.apsusc.2017.08.075
26. Liou TH (2010) Development of mesoporous structure and high adsorption capacity of biomass-based activated carbon by phosphoric acid and zinc chloride activation. Chem Eng J 158:129–142. https://doi.org/10.1016/j.cej.2009.12.016
27. Ding S, Liu Y (2020) Adsorption of CO_2 from flue gas by novel seaweed-based KOH activated porous biochars. Fuel 260:116382. https://doi.org/10.1016/j.fuel.2019.116382
28. Huang GG, Liu YF, Wu XX, Cai JJ (2019) Activated carbons prepared by the KOH activation of a hydrochar from garlic peel and their CO_2 adsorption performance. New Carbon Mater 34:247–257. https://doi.org/10.1016/S1872-5805(19)60014-4
29. Al-Wabel M, Elfaki J, Usman A, Hussain Q (2009) Performance of dry water- and porous carbon-based sorbents for carbon dioxide capture. Environ Res 174:69–79. https://doi.org/10.1016/j.envres.2019.04.020
30. Dias JM, Alvim-Ferraz CM, Almeida MF, Sanchez-Polo JM (2007) Waste materials for activated carbon preparation and its use in aqueous-phase treatment: A review. J Environ Manag 85:833–846. https://doi.org/10.1016/j.jenvman.2007.07.031
31. Khuong DA, Nguyen HN, Tsubota T (2021) Activated carbon produced from bamboo and solid residue by CO_2 activation utilized as CO_2 adsorbents. Biomass Bioenergy 148:106039. https://doi.org/10.1016/j.biombioe.2021.106039
32. Yang J, Yue L, Hu X, Wang L, Zhao Y, Lin Y, Guo L (2017) Efficient CO_2 capture by porous carbons derived from coconut shell. Energy Fuels 31:4287–4293. https://doi.org/10.1021/acs.energyfuels.7b006

33. Wu R, Ye Q, Wu K, Wang L, Dai H (2021) Highly efficient CO2 adsorption of corn kernel-derived porous carbon with abundant oxygen functional groups. J CO2 Util 51:101620. https://doi.org/10.1016/j.jcou.2021.101620
34. Ismail IS, Rashidi NA, Yusup S (2021) Production and characterization of bamboo-based activated carbon through single-step H_3PO_4 activation for CO2 capture. Environ Sci Pollut Res 29:12434–12440. https://doi.org/10.1007/s11356-021-15030-x
35. Yan M, Zhou Z, Zheng R, Jiang J, Feng H, Yu C, Zhu G, Hantoko D (2021) Low-temperature sintering behavior of fly ash from hazardous waste incinerator: Effect of temperature and oxygen on ash properties. J Environ Chem Eng 9:105261. https://doi.org/10.1016/j.jece.2021.105261
36. Hughes C, (1998) Monograph of Leucaena (Leguminosae-Mimosoideae), Systematic botany monographs, 55:1–5. ISBN 978–0–912861–55–5
37. Mallesh D, Anbarasan J, Mahesh Kumar P, Upendar K, Chandrashekar P, Rao BVSK, Lingaiah N (2020) Synthesis, characterization of carbon adsorbents derived from waste biomass and its application to CO_2 capture. Appl Surf Sci 530:147226–147232. https://doi.org/10.1016/j.apsusc.2020.147226
38. Kumar A, Mohan Jena H (2016) Preparation and characterization of high surface area activated carbon from Fox nut (Euryale ferox) shell by chemical activation with H_3PO_4. Results Phys 6:651–658. https://doi.org/10.1016/j.rinp.2016.09.012
39. Juarez-Galan J, Silvestre-Albero MA, Silvestre-Albero J, Rodríguez-Reinoso F (2009) Synthesis of activated carbon with highly developed ‘‘mesoporosity”. Microporous Mesoporous Mater 117:519–521. https://doi.org/10.1016/j.micromeso.2008.06.011
40. Beckert M, Menzel M, Tolle FJ, Bruchmann B, Mulhaupt R (2015) Nitrogenated graphene and carbon nanomaterials by carbonization of polyfurfuryl alcohol in the presence of urea and dicyandiamide. Green Chem 17:1032–1037. https://doi.org/10.1039/C4GC01676A
41. Hong K, Qie L, Zeng R, Yi Z, Zhang W, Wang D, Yin W, Wu C, Fan Q, Huang WXY (2014) Biomass derived hard carbon used as a high performance anode material for sodium ion batteries. J Mater Chem A 32:12733–12738. https://doi.org/10.1039/C4TA02068E
42. Singh G, Lakhi SK, Ramadass KCI, Vinu A (2019) High-performance biomass-derived activated porous biocarbons for combined pre- and post-combustion CO_2 capture, ACS sustainable. Chem Eng 7:7412–7420. https://doi.org/10.1021/acssuschemeng.9b00921
43. Datsyuk V, Papagelis K, Parthenios J, Tasis D, Siokou A, Kallitsis I, Galiotisa C (2018) Chemical oxidation of multiwalled carbon nanotubes. Carbon 46:833–840. https://doi.org/10.1016/j.carbon.2008.02.012
44. Padmakar D, Surendar M, Chandrashekar P, Lingaiah N (2020) A highly stable and efficient Co–Mg–Sr mixed oxide catalysts for hydrogen production from glycerol steam reforming. Catal Lett 150:2734–2743. https://doi.org/10.1007/s10562-020-031814
45. Li J, Michalkiewicz B, Min J, Ma C, Chen X, Gong J, Mijowsk E, Tang T (2019) Selective preparation of biomass-derived porous carbon with controllable pore sizes toward highly efficient CO_2 capture. Chem Eng J 360:250–259. https://doi.org/10.1016/j.cej.2018.11.204
46. Li D, Zhou J, Wang Y, Tian Y, Wei L, Zhang Z, Qiao Y, Li J (2019) Effects of activation temperature on densities and volumetric CO_2 adsorption performance of alkali-activated carbons. Fuel 238:232–239. https://doi.org/10.1016/j.fuel.2018.10.122
47. Basu S, Ghosh G, Saha S (2018) Adsorption characteristics of phosphoric acid induced activation of bio-carbon: Equilibrium, kinetics, thermodynamics and batch adsorber design, Process Saf. Environ Prot 117:125–142. https://doi.org/10.1016/j.psep.2018.04.015
48. Michele LB, Patrícia P, Janaína J, Daniele P, Aline D, Marcelo G (2017) Preparation and characterization of a metal-rich activated carbon from CCA-treated wood for CO_2 capture. Chem Eng J 321:614–621. https://doi.org/10.1016/j.cej.2017.04.004
49. Kim DG, Tae-Hoon K, Seok-Oh K (2022) Enhanced catalytic activity of a coal-based powdered activated carbon by thermal treatment. Water 14:3308–3320. https://doi.org/10.3390/w14203308
50. Kaur B, Gupta RK, Bhunia H (2019) Chemically activated nanoporous carbon adsorbents from waste plastic for CO_2 capture: Breakthrough adsorption study. Microporous Mesoporous Mater 282:146–158. https://doi.org/10.1016/j.micromeso.2019.03.025
51. Sivaraman B, Raja Sekhar BN, Nair BG, Hatode V, Mason NJ (2013) Infrared spectrum of formamide in the solid phase. Spectrochim Acta A Mol Biomol Spectrosc 105:238–244. https://doi.org/10.1016/j.saa.2012.12.039
52. Singh G, Lakhi KS, Sil S, Bhosale SV, Kim IY, Albahily K, Vinu A (2019) Biomass derived porous carbon for CO_2 capture. Carbon 148:164–186. https://doi.org/10.1016/j.carbon.2019.03.050
53. Jang E, Wan Choi S, Hong SM, Shin S, Lee KB (2018) Development of a cost-effective CO_2 adsorbent from petroleum coke via KOH activation. Appl Surf Sci 429:62–71. https://doi.org/10.1016/j.apsusc.2017.08.075
54. Fierro V et al (2006) Kraft lignin as a precursor for microporous activated carbons prepared by impregnation with ortho-phosphoric acid: Synthesis and textural characterization. Microporous Mesoporous Mater 92:243–250. https://doi.org/10.1016/j.micromeso.2006.01.013
55. Li J, Michalkiewicz B, Min J, Ma C, Chen X, Gong J, Mijowska E, Tang T (2019) Selective preparation of biomass-derived porous carbon with controllable pore sizes toward highly efficient CO_2 capture. Chem Eng J 360:250–259. https://doi.org/10.1016/j.cej.2018.11.204
56. Basu S, Ghosh G (2018) Adsorption characteristics of phosphoric acid induced activation of bio-carbon: equilibrium, kinetics, thermodynamics and batch adsorber design. Process Saf Environ 117(2018):125–142. https://doi.org/10.1016/j.psep.2018.04.015
57. Singh G, Ramadass K, Lee JM, Ismail IS, Singh M, Bansal V, Yang JH, Vinu A (2019) Convenient design of porous and heteroatom self-doped carbons for CO_2 capture. Microporous Mesoporous Mater 287:1–8. https://doi.org/10.1016/j.micromeso.2019.05.042
58. Chiang YC, Juang RS (2017) Surface modifications of carbonaceous materials for carbon dioxide adsorption: A review. J Taiwan Inst Chem Eng 71:214–234. https://doi.org/10.1016/j.jtice.2016.12.014
59. Prahas D, Kartika Y, Indraswati N, Ismadji S (2008) Activated carbon from jackfruit peel waste by H_3PO_4 chemical activation: Pore structure and surface chemistry characterization. Chem Eng J 140:32–42. https://doi.org/10.1016/j.cej.2007.08.032
60. Nilantha P, Mietek J (2013) Importance of small micropores in CO_2 capture by phenolic resin-based activated carbon spheres. J Mater Chem A 1:112–116. https://doi.org/10.1039/c2ta00388k
61. Silvestre-Albero J, Wahby A, Sepulveda-Escribano A, Martinez-Escandell M, Kaneko K, Rodriguez-Reinoso F (2011) Ultrahigh CO_2 adsorption capacity on carbon molecular sieves at room temperature. Chem Commun 47:6840–6842. https://doi.org/10.1039/C1CC11618E
62. Sevilla M, Antonio Fuerte B (2011) Sustainable porous carbons with a superior performance for CO_2 capture, energy environ. Sci 4:1765–1771. https://doi.org/10.1039/C0EE00784F
63. Wahby A, Ramos-Fernandez JM, Martinez-Escandell MA, Sepulveda-Escribano J, Silvestre-Albero F (2010) High-surface-area carbon molecular sieves for selective CO_2 adsorption. Chemsuschem 3:974–981. https://doi.org/10.1002/cssc.201000083

64. Zhanga S, Zhoua Q, Jianga X, Yaoa L, Jianga W, Xiea R (2019) Preparation and evaluation of nitrogen-tailored hierarchical meso-/micro-porous activated carbon for CO_2 adsorption. Environ Technol 41:3544–3553. https://doi.org/10.1080/09593330.2019.1615131
65. Wei H, Deng S, Hu B, Chen Z, Wang B, Huang J, Yu G (2012) Granular bambooderived activated carbon for high CO2 adsorption: the dominant role of narrow micropores. Chemsuschem 5:2354–2360. https://doi.org/10.1016/j.cej.2015.07.055
66. Turkan K (2021) Hydrogen storage characteristics of bio-based porous carbons of different origin: a comparative review. Int J Energy Res. https://doi.org/10.1002/er.7130
67. Turkan K, Sefa K (2010) Sulfur dioxide adsorption isotherms and breakthrough analysis on molecular sieve 5A zeolite. Chem Eng Commun 190:1041–1054. https://doi.org/10.1080/00986440302103
68. Wei H, Deng S, Hu B, Chen Z, Wang B, Huang J, Yu G (2012) Granular bamboo-derived activated carbon for high CO_2 adsorption: the dominant role of narrow micropores. Chemsuschem 5:2354–2360. https://doi.org/10.1002/cssc.201200570
69. Sevilla M, Falco C, Titirici MM, Fuertes AB (2012) High-performance CO_2 sorbents from algae. RSC Adv 2:12792–12797. https://doi.org/10.1039/c2ra22552b
70. Diez N, Alvarez P, Granda M, Blanco C, Santamaria R (2015) N-enriched ACF from coal-based pitch blended with urea-based resin for CO_2 capture. Microporous Mesoporous Mater 201:10–16. https://doi.org/10.1016/j.micromeso.2014.08.054
71. Ismail S, Singh G, Smith P, Kim S, Joseph YJH, S, Yusup S, Singh M, Siddulu VB, Talapaneni N, Vinu A, (2020) Oxygen functionalized porous activated biocarbons with high surface area derived from grape marc for enhanced capture of CO_2 at elevated pressure. Carbon 160:113–124. https://doi.org/10.1016/j.carbon.2020.01.008
72. Mutyala S, Jonnalagadda M, Mitta H, Gundeboyina R (2019) CO_2 capture and adsorption kinetic study of amine-modified MIL-101 (Cr). Chem Eng Res Des 143:241–248. https://doi.org/10.1016/j.cherd.2019.01.020
73. Wang J, Li M, Lu P, Ning P, Wang Q (2020) Kinetic study of CO_2 capture on ternary nitrates modified MgO with different precursor and morphology. Chem Eng J 39:123752. https://doi.org/10.1016/j.cej.2019.123752
74. Ello AS, de souza L.K.C., Trokourey A, Jaroniec M, (2013) Coconut shell-based microporous carbons for CO_2 capture. Microporous Mesoporous Mater 180:280–283. https://doi.org/10.1016/j.micromeso.2013.07.008
75. Nelson KM, Mahurin SM, Mayes RT, Williamson B, Teague CM, Binder AJ, Baggetto L, Veith GM, Dai S (2016) Preparation and CO_2 adsorption properties of soft-templated mesoporous carbons derived from chestnut tannin precursors. Microporous Mesoporous Mater 222:94–103. https://doi.org/10.1016/j.micromeso.2015.09.050
76. Li D, Tian Y, Li L, Li J, Zhang H (2015) Production of highly microporous carbons with large CO_2 uptakes at atmospheric pressure by KOH activation of peanut shell char. Porous Mater 22:1581–1588. https://doi.org/10.1007/s10934-015-0041-7
77. Gonzalez A, Plaza M, Rubiera F, Pevida C (2013) Sustainable biomass-based carbon adsorbents for post-combustion CO_2 capture. Chem Eng J 230:456–465. https://doi.org/10.1016/j.cej.2013.06.118
78. Ello AS, De Souza LK, Trokourey A, Jaroniec M (2013) Development of microporous carbons for CO_2 capture by KOH activation of African palm shells. J CO2 Util 2:35–38. https://doi.org/10.1016/j.jcou.2013.07.003
79. Singh G, Kim IY, Lakhi KS, Srivastava P, Naidu R, Vinu A (2017) Single step synthesis of activated bio-carbons with a high surface area and their excellent CO_2 adsorption capacity. Carbon 116:448–455. https://doi.org/10.1016/j.carbon.2017.02.015